

SOLAR NEUTRINO RATES, SPECTRUM, AND ITS MOMENTS : AN MSW ANALYSIS IN THE LIGHT OF SUPER-KAMIOKANDE RESULTS

Srubabati Goswami^{a *}, Debasish Majumdar^{a,b †}, and Amitava Raychaudhuri^{b ‡}

^a*Saha Institute of Nuclear Physics,
1/AF Bidhannagar, Calcutta 700 064, India.*

^b*Department of Physics, University of Calcutta,
92 Acharya Prafulla Chandra Road, Calcutta 700 009, India.*

ABSTRACT

We re-examine MSW solutions of the solar neutrino problem in a two flavor scenario taking (a) the results on total rates and the electron energy spectrum from the 1117-day SuperKamiokande (SK) data and (b) those on total rates from the Chlorine and Gallium experiments. We find that the SMA solution gives the best fit to the total rates data from the different experiments. One new feature of our analysis is the use of the moments of the SK electron spectrum in a χ^2 analysis. The best-fit to the moments is broadly in agreement with that obtained from a direct fit to the spectrum data and prefers a Δm^2 comparable to the SMA fit to the rates but the required mixing angle is larger. In the combined rate and spectrum analysis, apart from varying the normalization of the ^8B flux as a free parameter and determining its best-fit value we also obtain the best-fit parameters when correlations between the rates and the spectrum data are included and the normalization of the ^8B flux held fixed at its SSM value. We observe that the correlations between the rates and spectrum data are important and the goodness of fit worsens when these are included. In either case, the best-fit lies in the LMA region.

PACS Nos.: 14.60.Pq, 26.65.+t, 12.15.Ff

*E-mail address: sruba@tnp.saha.ernet.in

†E-mail address: debasish@tnp.saha.ernet.in

‡E-mail address: amitava@cubmb.ernet.in

1 Introduction

There is now strong evidence in support of an oscillatory behavior of neutrinos. The results on atmospheric neutrinos from SuperKamiokande [1] find a comprehensive explanation in terms of oscillations, indicating a non-zero neutrino mass. This result and the solar neutrino problem, which has been held as a signal for neutrino oscillations for long, have created much excitement in the community.

In this paper we examine the latest solar neutrino data from SuperKamiokande [2] along with those from the radiochemical Chlorine and Gallium experiments assuming that MSW resonant flavor conversion [3] is operative. The above experiments have presented the measured arrival rates [4] which, in all the cases, are less than the predictions from the Standard Solar Model (SSM). In addition, SuperKamiokande (SK) has provided the observed electron energy distribution [2, 5]. We use these data to test the consistency of the MSW mechanism taken together with the SSM predictions in a two flavor scenario. There are several recent MSW analyses of the SK solar neutrino data [6] - [11]. Although the data fitting method followed in all of them is to minimize a χ^2 function, the details of the statistical procedure used vary among the different groups. In this work, we indicate two different ways of performing the statistical analysis for the spectrum and the combined rate and spectrum data and check the consistency of the best-fit values of the mass squared differences and the mixing angles so obtained. For the analysis of the spectrum results we explore the possibility of using its moments as variables for fitting the data. The main advantage of these moments is that they probe the shape of the spectrum in a manner independent of the ^8B flux normalization uncertainties. For the combined analysis of the rates and the spectrum, apart from the standard procedure of varying the ^8B flux normalization and treating these two sets of data as independent, we also adopt a second method which takes into account the correlations among the rates and the spectrum data.

In addition to the best-fit values of the oscillation parameters, we present the 99% C.L. and 90% C.L. allowed regions and the goodness of fit (g.o.f) of a particular solution. By g.o.f. is meant the probability that the χ^2 will exceed χ_{min}^2 . When presenting the allowed region we take χ_{min}^2 to be the value at the *global* minimum in that region¹. For the neutrino fluxes and the neutrino production positions within the sun we use the BP98 solar model [12]. We consider oscillation of ν_e to a sequential (ν_μ or ν_τ) neutrino.

This paper is organized as follows. In the next section we present the formulae for oscillation of neutrinos with the inclusion of matter effects both in the sun and during their passage through the earth. In section 3 we use the data on the total solar neutrino rates as measured at the Chlorine, Gallium, and SuperKamiokande (1117-day data) detectors to obtain the best-fit values of the neutrino mass splitting and the mixing angles. In section 4 we consider the electron energy spectrum observed at SuperKamiokande. Using the MSW predictions, we obtain the best-fit values from a direct fit to the data as well as from a fit to the normalized moments. In section 5 we use both the total rates data and the SK electron energy spectrum data to make a combined fit. As noted earlier, here we allow the normalization of the ^8B spectrum to vary and compare the results with those obtained

¹The other approach is to present the allowed regions with respect to the *local* minimum.

when the SSM prediction for this normalization is used, allowing the inclusion of correlations between the total rates and the observed spectrum *via* astrophysical uncertainties. We end in section 7 with a summary, discussions, and conclusions.

2 Oscillation Probability

In this work we restrict ourselves to the simplest case of mixing between two neutrino flavors. Assuming the neutrino mass eigenstates, ν_i , reaching the earth to be incoherent [13], the survival probability of an electron neutrino can be written as

$$P_{ee} = \sum_i P_{ei}^S P_{ie}^E, \quad (1)$$

where P_{ei}^S is the probability of an electron neutrino state to transform into the i -th mass state at the solar surface and P_{ie}^E is the conversion probability of the i -th mass state to the ν_e state after traversing the earth. One can express P_{ee} in terms of the day-time (i.e. no earth matter effect) probability P_{ee}^D as²

$$P_{ee} = P_{ee}^D + \frac{(2P_{ee}^D - 1)(\sin^2 \theta - P_{2e}^E)}{\cos 2\theta}, \quad (2)$$

where

$$P_{ee}^D = 0.5 + [0.5 - \Theta(E_\nu - E_A)X] \cos 2\theta_M \cos 2\theta, \quad (3)$$

Θ being the Heaviside function. θ is the mixing angle in vacuum and θ_M is the mixing angle in matter given by

$$\tan 2\theta_M = \frac{\Delta m^2 \sin 2\theta}{\Delta m^2 \cos 2\theta - 2\sqrt{2}G_F n_e E_\nu}. \quad (4)$$

Here n_e is the ambient electron density, E_ν the neutrino energy, and $\Delta m^2 (= m_2^2 - m_1^2)$ the mass squared difference in vacuum.

$$E_A = \Delta m^2 \cos 2\theta / 2\sqrt{2}G_F n_e|_{pr}, \quad (5)$$

gives the minimum ν_e energy that can encounter a resonance inside the sun, $n_e|_{pr}$ being the electron density at the point of production. X is the jump-probability between the mass eigenstates and for an exponential density profile, as is approximately the case in the sun, it is given by [15]

$$X = \frac{\exp[-\pi\gamma_R(1 - \cos 2\theta)] - \exp[-2\pi\gamma_R]}{1 - \exp[-2\pi\gamma_R]}, \quad (6)$$

where $\gamma_R = \gamma \cos 2\theta / \sin^2 2\theta$ and

$$\gamma = \frac{\pi}{4} \frac{\Delta m^2 \sin^2 2\theta}{E_\nu \cos 2\theta} \frac{1}{\left| \frac{d \ln n_e}{dr} \right|_{res}}. \quad (7)$$

²This expression is not applicable for maximal mixing ($\cos 2\theta = 0$) [14] and for this case we use eq. (1) directly.

For calculating P_{2e}^E in eq. (2) we treat the earth as a slab of constant density (4.5 gm/cc). We have verified that this is a reasonable approximation since the location of the SK detector ensures that only in a rather small fraction of the time does the neutrino pass through the denser core.

The definition of χ^2 used by us in the following sections is,

$$\chi^2 = \sum_{i,j} \left(F_i^{th} - F_i^{exp} \right) (\sigma_{ij}^{-2}) \left(F_j^{th} - F_j^{exp} \right). \quad (8)$$

Here $F_i^\xi = T_i^\xi / T_i^{BP98}$ where ξ is *th* (for the theoretical prediction with oscillations) or *exp* (for the experimental value) and T_i stand for the quantities being fit (total rates from different experiments, electron energy spectrum for different energy bins, etc.). The error matrix σ_{ij} contains the experimental errors, the theoretical errors and their correlations.

3 Total rates

In this section we perform an analysis of the total rates as measured at the various experiments. The data that we use for the total rates are given in Table 1. In particular, we use the 1117-day SK data. For the Ga experiments we take the weighted average of the SAGE and Gallex results. Because SK has better statistics we do not include the Kamiokande results.

Experiment	Chlorine	Gallium	SuperKamiokande
$\frac{\text{Observed Rate}}{\text{BP98 Prediction}}$	0.33 ± 0.029	0.562 ± 0.043	0.465 ± 0.015

Table 1: The ratio of the observed solar neutrino rates to the corresponding BP98 SSM predictions used in this analysis. The results are from Refs. [4] and [2]. For Gallium, the weighted average of the SAGE and Gallex results has been used.

To get the best-fit values of the parameters, we minimise a χ^2 function defined as in eq. (8). For evaluating the error matrix, σ_{ij} , we use the procedure described in [16]. Our best-fit results for the total rates are summarized in Table 2. These fits have 1 degree of freedom (3 experimental data points – 2 parameters). It is clear from this Table that the small mixing angle solution for the sequential neutrino case gives by far the best fit to the total rates data.

It is seen from Table 2 that the best-fit values obtained for the 1117-day data are not markedly different from those obtained for the 825-day data. This indicates that the best-fit points obtained from the analysis of total rates are quite robust and are not expected to change drastically with more data from SK. However, the quality of fit is quite sensitive to these small changes: the g.o.f. has become a little poorer for the SMA solution while for both the LMA and LOW solutions it has improved with the accumulation of more SK data.

In Fig. 1 we show the 99% C.L. and 90% C.L. contours in the $\sin^2 \theta - \Delta m^2$ plane for the MSW solution. There is no solution in the *dark side* ($\sin^2 \theta > 0.5$) from the analysis of total rates. Note that in [17] allowed regions were obtained in the dark side from the total rates

No. of days of SK running	Nature of Solution	Δm^2 in eV ²	$\sin^2 \theta$	χ_{min}^2	Goodness of fit
1117	SMA	5.19×10^{-6}	1.53×10^{-3}	0.30	58.38%
	LMA	1.42×10^{-5}	0.22	3.52	6.06%
	LOW	9.97×10^{-8}	0.38	6.64	.997%
825	SMA	5.33×10^{-6}	1.50×10^{-3}	0.06	80.64%
	LMA	1.40×10^{-5}	0.23	4.31	3.78%
	LOW	9.98×10^{-8}	0.38	7.39	0.65%

Table 2: The best-fit values of the parameters, χ_{min}^2 , and the g.o.f. for fits to the total rates of the different experiments. SMA, LMA, LOW stand for the Small Mixing Angle, Large Mixing Angle and Low mass-low χ^2 regions, respectively. The results for the earlier 825-day SK data (0.475 ± 0.015) are also presented for comparison.

analysis while in [18] no allowed region was found for $\theta > \pi/4$. We agree with [18]; a possible origin of this is that the same numerical density profile of the sun from BP98 has been used in these analyses. Our results for the total rates for the 1117 day data are in agreement with the analysis given in [19].

4 Observed spectrum and its moments

In addition to the total rates, SK has provided the number of events (normalized to the SSM prediction) in 18 electron recoil energy bins of width 0.5 MeV in the range 5.0 MeV to 14 MeV and a 19th bin which covers the events in the range 14 to 20 MeV [2]. The systematics of the first bin are still under study and for our analysis we do not use it.

4.1 Observed spectrum

In this subsection we present the results obtained by directly fitting the SK spectral data. The theoretical predictions are calculated bin by bin and in the fitting procedure, in addition to the neutrino mixing parameters Δm^2 and $\sin^2 \theta$, we also allow the absolute normalization of the ^8B flux, X_B , to vary³. The error matrix σ_{ij} used by us (see eq. (8)) is [8]

$$(\sigma_{ij}^2)_{sp} = \delta_{ij}(\sigma_{i,stat}^2 + \sigma_{i,uncorr}^2) + \sigma_{i,exp}\sigma_{j,exp} + \sigma_{i,cal}\sigma_{j,cal}, \quad (9)$$

where we have included the statistical error, the uncorrelated systematic errors and the energy-bin-correlated experimental errors [20] as well as those from the calculation of the shape of the expected spectrum [21]. Since we vary the normalization of the ^8B flux we do not include its astrophysical uncertainties separately.

The best-fit point from this analysis is found to be

³ $X_B = 1$, for the SSM.

- $\Delta m^2 = 2.29 \times 10^{-6} \text{ eV}^2$, $\sin^2 \theta = 0.009$, $X_B = 1.4$, $\chi_{min}^2 = 9.46$, g.o.f. = 85.23%.

For these values of Δm^2 and $\sin^2 \theta$, choosing $X_B = 1$, the data on total rates give a bad fit ($\chi^2 = 73.82$) as the high energy ${}^8\text{B}$ neutrinos get suppressed more than observed. For the spectrum fit this problem can be avoided by a high $X_B > 1$. Since the ${}^8\text{B}$ flux normalization is allowed to vary, a large range of Δm^2 and $\sin^2 \theta$ including the $\theta > \pi/4$ region remains allowed by the spectral data as is shown in Fig. 2. Only the area inside the contours is *disallowed* at 90% C.L. from spectral data analysis.

To further examine this mismatch between the fits to the total rates and those to the SK spectral data, in Fig. 3 we present the behavior of χ^2 as obtained from the spectral analysis if we keep the parameters $\sin^2 \theta$ and Δm^2 in the SMA, LMA, and LOW regions of the fit to the total rates. In Figs. 3(a), 3(b), and 3(c) are shown the variation of the χ^2 from the spectral data with $\sin^2 \theta$ lying in the SMA, LMA, and LOW regions respectively. For any chosen $\sin^2 \theta$, we let Δm^2 vary over the corresponding range permitted by the fit to the total rates at 99% C.L. (from Fig. 1) and plot the minimum value found. We consider two cases,

- the ${}^8\text{B}$ normalization is held fixed at its SSM value (solid curves)
- the ${}^8\text{B}$ normalization is permitted to vary (broken curves).

For Figs. 3(d), 3(e), and 3(f), the roles of $\sin^2 \theta$ and Δm^2 are interchanged. Fig. 3 indicates that if we allow the ${}^8\text{B}$ normalization to vary then the Δm^2 and $\sin^2 \theta$ allowed at 99% C.L. from the total rates are allowed at 90% C.L. from the spectral analysis.

Figs. 2 and 3 lead us to the conclusion that, at the present moment, the SK electron spectral data do not provide tight controls over the allowed parameter range.

4.2 Moments of spectrum

Since the absolute normalization of the ${}^8\text{B}$ flux is not precisely known, it is of interest to look for variables which probe neutrino oscillation effects in the data in a manner immune to this uncertainty. Normalized moments of the observed electron spectrum can be useful as one such set of variables [22, 23]. In practice, to compare with the data, it is convenient to standardize with respect to the SSM predictions by using

$$M_n = \frac{\sum_i \left[\frac{N(E_i)}{\{N(E_i)\}_{SSM}} \right] E_i^n}{\sum_i \left[\frac{N(E_i)}{\{N(E_i)\}_{SSM}} \right]}, \quad (10)$$

where E_i is the mean energy of the i -th bin and $N(E_i)$ is the number of events in this bin. Depending on whether the experimental or the theoretically predicted value of the variable is under consideration, $N(E_i)$ is obtained either from experiments or from the theoretical model under test. It is clear that these variables carry information about the shape of the neutrino spectrum which, if oscillations are operative, undergoes modification from the SSM prediction due to the energy dependence of the survival probability. It is obvious that the above moments are independent of the absolute normalization of the ${}^8\text{B}$ flux.

We have calculated the moments of the 1117-day data on the electron energy spectrum presented by SuperKamiokande [2]. These are presented in Table 3. The error in the higher

moments increases rapidly with the order and the ones beyond the sixth are not of much use.

Order of Moment	Value of Moment	Calculated Error in Moment
1	10.25	0.33
2	113.84	7.12
3	1356.59	164.34
4	17167.7	3616.65
5	228876.2	75981.0
6	3188064.0	1541763.0

Table 3: Moments of the observed electron energy spectrum and their calculated errors obtained from the SK (1117 days) data.

Using these variables in a χ^2 -analysis we find that fitting the first four moments results in the same best-fit values of Δm^2 and $\sin^2 \theta$ as those obtained using the first five or six moments. The best-fit region⁴ is found to be

- $\Delta m^2 = 6.94 \times 10^{-6} \text{ eV}^2$, $\sin^2 \theta = 0.007 - 0.010$, $\chi_{min}^2 = 0.0001$, g.o.f = 99.995%.

The very small value of χ_{min}^2 for this fit should not be regarded as a major success of the theory but rather reflects the large errors associated with the moments as obtained from the present data. It is gratifying that the best-fit values obtained by this method are in the same broad region as those from fitting the recoil electron energy spectrum.

5 Combined fits to rates and spectrum

In this section we present the results of the combined fit to the total rates and the spectrum data. We have performed this global fit by the following two methods:

- (a) We treat the rates and the electron spectrum data as independent. In this approach we vary the ^8B flux normalization as a free parameter.
- (b) We fix the ^8B flux normalization at the SSM value (=1) and include the correlations of the ^8B flux uncertainty between the rates and spectrum data. To our knowledge, this approach has not been pursued in any previous analysis.

⁴The χ^2 remains unchanged when $\sin^2 \theta$ is varied over the indicated range

5.1 Fits using the ^8B flux normalization as a free parameter

For this case the definition of χ^2 is,

$$\chi^2 = \sum_{i,j=1,3} (F_i^{th} - F_i^{exp}) (\sigma_{ij}^{-2}) (F_j^{th} - F_j^{exp}) + \sum_{i,j=1,18} (X_B R_i^{th} - R_i^{exp}) (\sigma_{ij}^{-2})_{sp} (X_B R_j^{th} - R_j^{exp}), \quad (11)$$

where the first term on the r.h.s is from the fit to the total rates and the second from that to the spectral data. As we allow the normalization of the ^8B flux to vary as a free parameter we switch off the SSM astrophysical uncertainties arising because of this component. Since it is the ^8B flux that enters the rates as well as the spectrum data, in this manner of fitting the data the correlations between the rates and the spectrum are absent; the error matrix is block diagonal and one can treat χ_{rate}^2 and $\chi_{spectrum}^2$ as independent. There are 18 ($= 21 - 3$) degrees of freedom in this case. The best-fit values we obtain are presented in Table 4.

Nature of Solution	Δm^2 in eV^2	$\sin^2 \theta$	X_B	χ_{min}^2	Goodness of fit
SMA	4.81×10^{-6}	5.92×10^{-4}	0.61	12.62	81.36%
LMA	1.82×10^{-5}	0.18	1.39	10.97	89.56%
LOW	1.0×10^{-7}	0.38	0.95	17.21	50.87%

Table 4: The best-fit values of the parameters, χ_{min}^2 , and the g.o.f. for fits to the total rates measured at the Cl, Ga, and SK detectors along with the electron energy spectrum from SK (1117 days) when the ^8B flux normalization factor X_B is allowed to vary.

In Fig. 4a we show the 99% and 90% C.L. allowed regions for the combined analysis of total rates and the observed electron spectrum. The best-fit points in these plots are obtained by varying X_B in addition to Δm^2 and $\sin^2 \theta$.

5.2 Fits including correlations between rates and spectrum *via* ^8B flux

For this case we include the correlations between the theory errors in the rate and the spectrum data. This comes through the ^8B flux, as it enters both. Since we include the SSM astrophysical uncertainties in the ^8B flux the normalization factor for it is held fixed at the SSM value. Now the individual χ^2 due to the spectrum and the rates cannot be summed independently and the combined χ^2 is defined as,

$$\chi^2 = \sum_{i,j=1,21} (F_i^{th} - F_i^{exp}) (\sigma_{ij}^{-2}) (F_j^{th} - F_j^{exp}), \quad (12)$$

where the σ_{ij} is now a 21×21 matrix defined in the following way,

- For $i, j = 1 \dots 3$

$$\sigma_{ij}^2 = (\sigma_{ij}^2)_{th} + (\sigma_{ij}^2)_{exp}, \quad (13)$$

where

$$(\sigma_{ij}^2)_{th} = \delta_{ij} \sum_{\alpha=1}^8 R_{\alpha i}^2 (\Delta C_{\alpha i})^2 + \sum_{\alpha, \beta=1}^8 R_{\alpha i} R_{\beta j} \sum_{k=1}^{e11} a_{\alpha k} a_{\beta k} (\Delta \ln X_k)^2. \quad (14)$$

where the first term is due to the cross-section uncertainties and the second term (σ_{ap}) is due to the astrophysical uncertainties [16]. The off-diagonal elements in the error matrix come through σ_{ap} . $R_{\alpha i}$ denotes the contribution of the α -th source to the rate of the i -th experiment. $a_{\alpha k} = \delta \ln \phi_{\alpha} / \delta \ln X_k$, where $\delta \ln \phi_{\alpha}$ is the error in the α -th component of the spectrum due to the input parameter X_k [12].

- For $i = 4 \dots 21$ and $j = 1 \dots 3$

$$\sigma_{ij}^2 = \sum_{\alpha=1}^8 R_{s_{Bi}} R_{\alpha j} \sum_{k=1}^{11} a_{s_{Bk}} a_{\alpha k} (\Delta \ln X_k)^2. \quad (15)$$

- For $i = 1 \dots 3$ and $j = 4 \dots 21$

$$\sigma_{ij}^2 = \sum_{\alpha=1}^8 R_{\alpha i} R_{s_{Bj}} \sum_{k=1}^{11} a_{\alpha k} a_{s_{Bk}} (\Delta \ln X_k)^2. \quad (16)$$

- for $i = 4 \dots 21$ and $j = 4 \dots 21$

$$\sigma_{ij}^2 = (\sigma_{ij}^2)_{sp} + R_{s_{Bi}} R_{s_{Bj}} \sum_{k=1}^{11} a_{s_{Bk}} a_{s_{Bk}} (\Delta \ln X_k)^2. \quad (17)$$

In this case the number of degrees of freedom is 19 ($= 21 - 2$). The χ_{min}^2 and the best-fit values we obtain are shown in Table 5.

Nature of Solution	Δm^2 in eV ²	$\sin^2 \theta$	χ_{min}^2	Goodness of fit
SMA	5.15×10^{-6}	4.8×10^{-4}	15.72	67.58%
LMA	2.23×10^{-5}	0.25	14.53	75.19%
LOW	1.00×10^{-7}	0.38	17.62	54.79%

Table 5: The best-fit values of the parameters, χ_{min}^2 , and the g.o.f. for fits to the total rates measured at the Cl, Ga, and SK detectors along with the electron energy spectrum from SK (1117 days). In this case the ^8B flux is chosen as in the SSM and the correlation between the rates and the spectrum due to astrophysical uncertainties is included.

We find that the fits are of poorer quality in this case as compared to the previous one.

In Fig. 4b we show the 99% and 90% C.L. allowed regions for the combined analysis of total rates and the observed electron spectrum for MSW conversion to sequential neutrinos including the correlations between the rates and the spectrum due to the astrophysical uncertainties of the ${}^8\text{B}$ flux normalization.

6 Summary, Discussions, and Conclusions

In this paper we have performed a detailed χ^2 -analysis of the latest SK solar neutrino data together with the results from the Cl and Ga experiments in terms of two-generation MSW conversions of ν_e to sequential (ν_μ, ν_τ) neutrinos.

Compared to the recent analyses in the literature [6]-[11] there are two new features in our analysis.

- We fit the observed electron energy spectrum data in two different ways, exploring for the first time, the use of moments of the energy spectrum in a χ^2 -analysis.
- The combined fits to the total rates and spectral data are also performed in two different manners. In the first, the ${}^8\text{B}$ flux normalization is used as a free parameter while in the other the SSM normalization is chosen for it and correlations between the rates and spectral data due to astrophysical uncertainties of the ${}^8\text{B}$ flux are included.

We find that the two-generation MSW scenario can well explain the data on total rates. The solution in the SMA (Small Mixing Angle) region is preferred over the other possibilities although the quality of the fit is poorer as compared to the one obtained using the 825-day SK data.

The best-fit from the spectrum data comes in a region disallowed from the total rates. In this region the ${}^8\text{B}$ neutrinos are suppressed much more than required by the rates data. For the analysis of the spectrum, the absolute normalization of the ${}^8\text{B}$ flux, X_B , has been permitted to be greater than unity, thus effectively compensating the shortfall. We have explored the use of normalized moments of the observed electron energy spectrum to signal MSW resonant flavour conversion. These variables are independent of the absolute normalization of the ${}^8\text{B}$ flux and probe the effect of oscillations on the spectral shape. This procedure is somewhat handicapped by the large errors on the moments calculated from the present data. However, the best-fit values obtained by the two methods are more or less in agreement.

Similarly, for the two methods followed in the combined χ^2 analysis of the rates and time averaged spectrum data, the best-fit values are not much different. The first approach gives a better fit because we utilise the freedom of varying the ${}^8\text{B}$ flux normalization. We remark that in the combined analysis, where the ${}^8\text{B}$ normalization is held fixed at the SSM value, the correlations between the rates and the spectrum data are found to be important and thus one should use caution regarding results obtained treating these as independent. For both methods, the best-fit from the combined analysis falls in the LMA region. Compared to the rates analysis the goodness of fit of the LOW(SMA) region increases(decreases). With the inclusion of the day-night dependence of the data the goodness of fit in the SMA region worsens further [2].

In this work we have not included the new GNO result [24] which is consistent with the Gallex and SAGE data. Thus its inclusion is not expected to affect the conclusions drastically. For illustration we give below the results of the global analysis of rates and spectrum including the GNO data. We take the weighted average of Gallex and GNO and treat SAGE as a separate experiment. The best-fit values and χ_{min}^2 that we get are:

- $\sin^2 \theta = 5.26 \times 10^{-4}$, $\Delta m^2 = 5.28 \times 10^{-6} \text{ eV}^2$, $X_B = 0.61$, $\chi_{min}^2 = 12.73$, g.o.f = 85.21% (SMA)
- $\sin^2 \theta = 0.18$, $\Delta m^2 = 2.48 \times 10^{-5} \text{ eV}^2$, $X_B = 1.39$, $\chi_{min}^2 = 11.55$, g.o.f = 90.39% (LMA)
- $\sin^2 \theta = 0.41$, $\Delta m^2 = 9.39 \times 10^{-8} \text{ eV}^2$, $X_B = 0.89$, $\chi_{min}^2 = 19.85$, g.o.f = 40.34% (LOW)

Thus the global best-fit continues to be in the LMA region.

In conclusion, we have probed the most recent solar neutrino data on total rates and the observed electron energy spectrum at SK from various angles within the framework of MSW flavour conversion. We find good fits in some situations but a degree of uncertainty still remains since different fits do not prefer the same values of the parameters. More data from the running and new experiments, it is hoped, will further sharpen the results in the near future.

Acknowledgements

D.M. and A.R. are partially supported by the Eastern Centre for Research in Astrophysics, India. A.R. also acknowledges a research grant from the Council of Scientific and Industrial Research, India. We would like to thank Sandhya Choubey for pointing out an error in one of our computer codes and J.W.F. Valle for drawing our attention to the updated analysis in [8]. S.G. would like to thank Plamen Krastev for many helpful correspondences.

References

- [1] Y. Fukuda *et al.*, (The Super-Kamiokande collaboration), *Phys. Rev. Lett.* **81**, 1562 (1998).
- [2] The results presented at the Neutrino2000 meeting can be found at <http://nu2000.sno.laurentian.ca>.
- [3] L. Wolfenstein, *Phys. Rev.* **D34**, 969 (1986); S.P. Mikheyev and A.Yu. Smirnov, *Sov. J. Nucl. Phys.* **42(6)**, 913 (1985); *Nuovo Cimento* **9c**, 17 (1986).
- [4] B.T. Cleveland *et al.*, *Nucl. Phys. B (Proc. Suppl.)* **38**, 47 (1995); Y. Fukuda *et al.*, (The Kamiokande collaboration), *Phys. Rev. Lett.* **77**, 1683 (1996); W. Hampel *et al.*, (The Gallex collaboration), *Phys. Lett.* **B388**, 384 (1996); J.N. Abdurashitov *et al.*, (The SAGE collaboration), *Phys. Rev. Lett.* **77**, 4708 (1996).

- [5] Y. Fukuda *et al.*, (The Super-Kamiokande collaboration), *Phys Rev. Lett.* **81**, 1158 (1998); **82**, 2430 (1999).
- [6] Y. Suzuki, Talk given at the Lepton-Photon Symposium '99, <https://www.sldnt.slac.stanford.edu/lp99/db/program.asp>.
- [7] J.N. Bahcall, P.I. Krastev, and A.Yu. Smirnov, *Phys. Rev.* **D58**, 096016 (1998).
- [8] M.C. Gonzalez-Garcia, P.C. de Holanda, C. Peña-Garay, and J.W.F. Valle, hep-ph/9906469, *Nucl. Phys.* **B573**, 3 (2000).
- [9] J.N. Bahcall, P.L. Krastev, and A.Yu. Smirnov, *Phys. Lett.* **B477**, 401 (2000).
- [10] G.L. Fogli *et al.*, hep-ph/9912231, *Phys. Rev.* **D62** 013002 (2000).
- [11] C. Giunti, M.C. Gonzalez-Garcia, and C. Peña-Garay, hep-ph/0001101, *Phys. Rev.* **D62** 013005, (2000).
- [12] J.N. Bahcall, S. Basu, and M. Pinsonneault, *Phys. Lett.* **B433**, 1 (1998).
- [13] A. Yu. Smirnov and A. Dighe, hep-ph/9903329 and references therein.
- [14] Alan H. Guth, Lisa Randall, Mario Sena, *JHEP* 9908, 018, (1999).
- [15] S.T. Petcov, *Phys. Lett.* **B200**, 373 (1988).
- [16] G.L. Fogli and E. Lisi, *Astropart. Phys.* **3**, 185 (1995).
- [17] Andre de Gouvea, A. Friedland, and H. Murayama, hep-ph/0002064.
- [18] M.C. Gonzalez-Garcia and C. Peña-Garay, hep-ph/0002186, *Phys. Rev.* **D62**, 031301, (2000).
- [19] M.C. Gonzalez-Garcia, <http://nu2000.sno.laurentian.ca>.
- [20] For a discussion on the sources of the various errors see the second reference of [5].
- [21] J.N. Bahcall *et al.*, *Phys. Rev.* **D54**, 411 (1996).
- [22] D. Majumdar and A. Raychaudhuri, *Phys. Rev.* **D60**, 053001 (1999).
- [23] J.N. Bahcall and E. Lisi, *Phys. Rev.* **D54**, 5417 (1996); S.M. Bilenky and C. Giunti, *Phys. Lett.* **B311**, 179 (1993); *ibid.* **B320**, 323 (1994); G. Fiorentini, M. Lissia, G. Mezzorani, M. Moretti, and D. Vignaud, *Phys. Rev.* **D49**, 6298 (1994); W. Kwong and S.P. Rosen, *ibid.* **D51**, 6159 (1995).
- [24] M. Altmann *et al.*, (The GNO collaboration), hep-ex/0006034.

Figure Captions

Fig 1. The 99% and 90% C.L. allowed regions in the $\Delta m^2 - \sin^2 \theta$ plane from the analysis of total rates for the Chlorine and Gallium detectors and the 1117-day data from SK. The best-fit points are also indicated. The dark side ($\sin^2 \theta > 0.5$) is indicated by the dashed line.

Fig 2. The 90% C.L. allowed region in the $\Delta m^2 - \sin^2 \theta$ plane from the 1117-day SK recoil electron spectrum data. The regions enclosed by the contours are *disallowed*. The best-fit point is indicated. The dark side is to the right of the dashed line.

Fig. 3. The minimum χ^2 for fits to the SK 1117-day recoil electron spectrum as a function of $\sin^2 \theta$ (Δm^2) are shown in (a), (b), and (c) ((d), (e), and (f)) when the parameter ranges are determined by the 99% C.L. allowed regions in the SMA, LMA, and LOW fits respectively to the total rates data. The solid (broken) curves are obtained when X_B is held fixed at its SSM value (allowed to vary). The dash-dotted line indicates the 90% C.L. limit for 3 parameters. See text for more details.

Fig. 4. The 99% and 90% C.L. allowed region in the $\Delta m^2 - \sin^2 \theta$ plane from an analysis of the total rates from the Chlorine and Gallium detectors and the 1117-day SK data taken together with the 1117-day SK recoil electron spectrum. The normalization of the ^8B flux is chosen as a free parameter in (a) and held fixed at the SSM value in (b). In (b) the correlations between the rates and spectrum data are included. The best-fit points are also indicated. The dark side corresponds to the right of the dashed line.

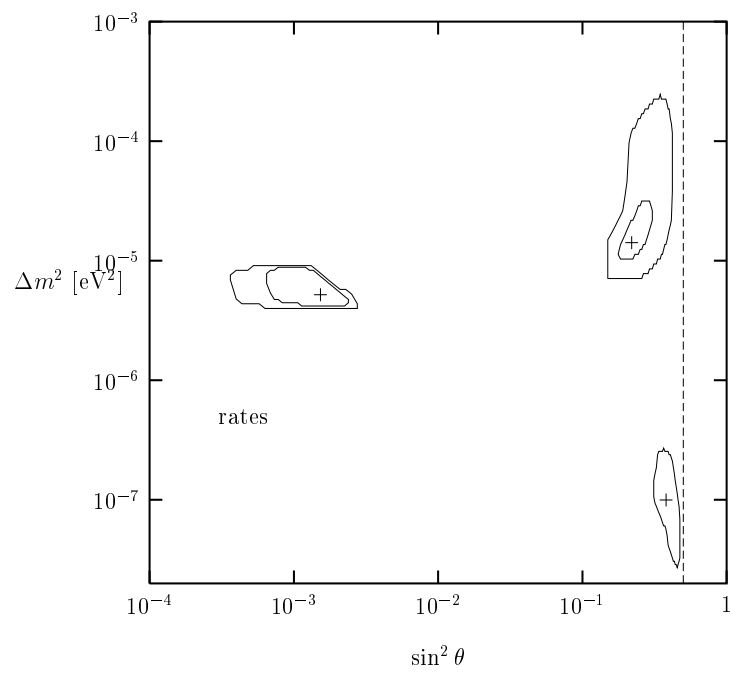


Fig. 1

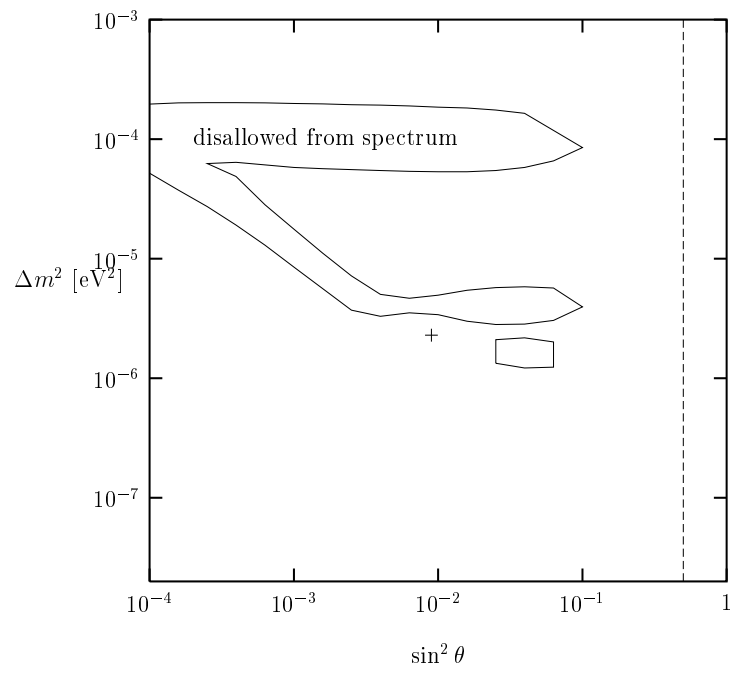


Fig. 2

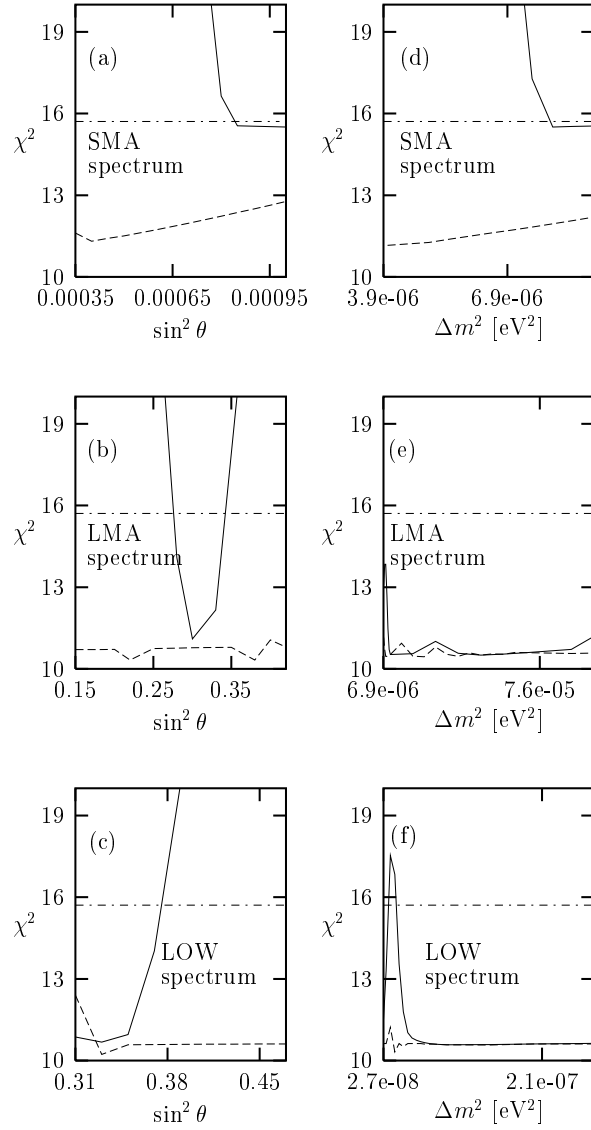


Fig. 3

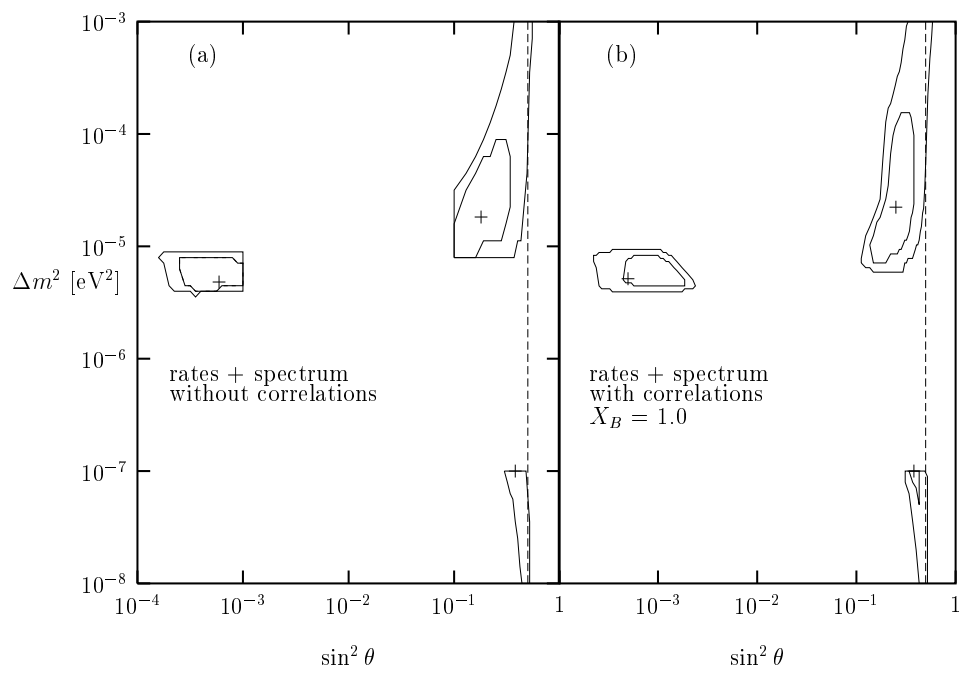


Fig. 4